Hindawi Publishing Corporation
International Journal of Photoenergy
Volume 2012, Article ID 759306, 9 pages
doi:10.1155/2012/759306

Research Article

Mechanistic Study of Visible-Light-Induced Photodegradation of 4-Chlorophenol by $TiO_{2-x}N_x$ with Low Nitrogen Concentration

Guangfeng Shang,[1] Hongbo Fu,[1] Shaogui Yang,[2] and Tongguang Xu[3]

[1] *Department of Environmental Science and Engineering, Fudan University, Shanghai 200433, China*
[2] *State Key Laboratory of Pollution Control and Resource Reuse, School of the Environment, Nanjing University, Nanjing 210046, China*
[3] *Department of Chemistry, Tsinghua University, Beijing 100084, China*

Correspondence should be addressed to Hongbo Fu, fuhb@fudan.edu.cn

Received 7 April 2011; Accepted 3 May 2011

Academic Editor: Jiaguo Yu

$TiO_{2-x}N_x$ powders with low N-doping concentrations ($0.021 < x < 0.049$) were prepared by annealing commercial TiO_2 (P-25) under an NH_3 flow at 550°C. Regardless of UV or visible case, the photoactivities of the samples decreased as x increased, and $TiO_{1.979}N_{0.021}$ showed the highest activity for the 4-chlorophenol (4-CP) decomposition under the visible-light irradiation. The visible-light response for N-doped TiO_2 could arise from an N-induced midgap level, formed above the valence band (O 2p). Electron spin resonance (ESR) measurements and the radical scavenger technologies gave the combined evidence that the active species (•OH and $O_2•^-$) are responsible for the photodecomposition of 4-CP over $TiO_{2-x}N_x$ under the visible irradiation. A possible photocatalytic mechanism was discussed in detail.

1. Introduction

Semiconductor photocatalysis has been the focus of numerous investigations because of its application for the destruction of chemical contaminants and water splitting [1–5]. Among all the materials, TiO_2 remains the most promising owing to its superior photoreactivity, high corrosion resistance, and nonhazardous nature. Even so, the poor solar efficiency (maximum 5%) has hindered the commercialization of this technology [6–8]. Various approaches have been attempted to enhance the visible-light utilization of TiO_2. A classical example is the doping of TiO_2 with transition-metal elements [9, 10]. However, the doped materials have been shown to suffer from thermal instability, and the metal centers act as electron traps, which reduces the photocatalytic efficiency. Dye sensitization in photochemical systems has also been explored extensively [11, 12]. Dyes possessing carboxylate or hydroxyl functions, in particular, interact with the surface of TiO_2 particles, thereby providing the path for electron-transfer from the excited dye adsorbate to the semiconductor. Unfortunately, this technology cannot be practically used for detoxification of waste water since the photosensitizers may be gradually photodegraded and become less effective.

Recently, the band gap of TiO_2 has been narrowed successfully by doping with nonmetal cations, by replacing lattice oxygen with B, C, N, or S dopants [13–16]. It is widely recognized that anionic nonmetal dopants may be more appropriate for the extension of photocatalytic activity into the visible-light region, because the related impurity states are supposed to be close to the valence band maximum [17]. Furthermore, the position of the conduction band minimum, which must be kept at the level of the H2/H2O potential, when TiO_2 is used for the photoelectrolysis of water into hydrogen and oxygen, is not affected [17].

Among all the nonmetal cations, substitutional N-doping was found to be particularly effective in decreasing the band gap of TiO_2 through the mixing of N and O 2p states. The presence of nitrogen doping extends the optical absorption of TiO2 to the visible-light spectrum and enhances the visible-light-driven photocatalysis [18–24]. Generally, N-doped TiO_2 samples have been produced by

different preparative procedures: (i) treating TiO_2 powder with NH3 gas at high temperature (>500°C) followed by partial reoxidation in air [15, 17]; (ii) via "nitridation" of TiO_2 colloidal nanoparticles with alkylammonium salts at room temperature [18]; (iii) hydrolysis of NHx/TiO_2 mixtures to gain powder samples [20]; (iv) to produce carbon-substituted N-doped sample by a flame pyrolysis at high temperature [25]. The various N-doped TiO_2 catalysts have been applied to bleach methylene blue [18], split water [23], and oxidatively degrade 2-propanol [26], 4-CP [19], acetone vapors [27], and for the photokilling of harmful pathogens as well as peroxidation of the cell membrane of biomolecules [20]. Indeed, the visible-light-induced photocatalysis of the N-doped TiO_2 is effective.

However, it is quite debatable as to the origin of the visible-light responses for N-doped TiO_2 to date. On the basis of a theoretical analysis, Han et al. [15] suggested that visible-light responses for N-doped TiO_2 arose from band narrowing by mixing of N 2p and O 2p orbitals. Irie et al. [26] insisted that visible light sensitivity of N-doped TiO_2 was due to an isolated N 2p state rather than the narrowing of the band gap. Further, Lindgren et al. [28] reported that N 2p was situated close to the valence band maximum by using the photoelectrochemical measurements and that the conduction band edge remained unchanged by N-doping. Ihara et al. [27] argued that the oxygen vacancies were contributed to the Vis activity and the doped N atoms only enhance the stabilization of these oxygen vacancies.

Another question relates to the photodegradation mechanism involved in the N-doped TiO_2 photocatalysis. It has been reported that a variety of organic compounds are mineralized into CO_2 and inorganic species on N-doped TiO_2 under visible-light illumination [18, 19, 26]. However, it still remains conjectural whether the certain product comes from a direct reaction with photogenerated holes or via reactions with surface intermediates of the water photooxidation reaction. It is thus quite difficult to get definite conclusions on the reaction mechanism. An examination of the formation of active oxygen species can provide useful information about the fate of the valence hole and the conduction electrons, and lead to a greater understanding of the visible-induced photocatalysis by N-doped TiO_2 in general.

In the previous work, we have already observed the photocatalytic process mediated by N-doped TiO_2 using an ESR technique [29]. In this report, to further observe the mechanism of this photocatalytic system, N-doped TiO_2 powders were firstly prepared by annealing the commercial P-25 (TiO_2) in NH3 flow at 550°C. The samples were characterized by X-ray photoelectron spectroscopy (XPS), X-ray diffraction (XRD), and UV-Vis diffused reflection spectrum (DRS). 4-CP decomposition was used as a probe reaction to evaluate the photocatalytic activities of these powders under UV and Vis irradiation. The formation of active oxygen species was detected by spin-trap electron spin resonance (ESR) techniques and the radical scavenger technologies to provide an overall understanding of the reaction mechanisms.

2. Experimental Section

2.1. Materials. Commercial P-25 (Degussa, $50\,m^2\,g^{-1}$, 75% rutile, and 25% anatase) was treated in a flow reactor system in an N_2 gas atmosphere (1 atm) at 550°C. For doping, the N_2 flow was replaced by NH_3 for 5~25 min after the target temperature had been reached. Subsequently, the crystals were kept in flowing N_2 for 1 h at 550°C and then cooled in flowing N_2. For comparison, undoped P-25 was also annealed under N_2 flow at 550°C for 25 min as a reference sample.

The spin trap 5, 5-dimethyl-1-pyrroline-N-oxide (DMPO) was kindly supplied. Stock solutions of DMPO in deaerated water were prepared under argon and stored in the dark bottles at –20°C. All chemicals were reagent grade and used without further purification. Deionized and doubly distilled water were used throughout this study.

2.2. Characterization. XPS analysis was obtained using a PHI 5300 ESCA instrument with an Al Ka X-ray source at a power of 250 W. The pass energy of the analyzer was set at 35.75 eV and the base pressure of the analysis chamber was $<3 \times 10^{-9}$ Torr. The binding energy scale was calibrated with respect to the C 1s peak of hydrocarbon contamination fixed at 285.0 eV. According to Irie et al. [26], the peak at 396 eV is derived from Ti-N bonds. Therefore, the x values (nitrogen concentrations) in $TiO_{2-x}N_x$ were estimated by comparing to the product of the 396 eV peak area multiplied by the nitrogen sensitivity factor to the product of the 531 eV peak area (O 1s, Ti–O bonds) multiplied by the oxygen sensitive factor. XRD patterns of the powders were recorded by a Bruker D8 Advance X-ray diffractometer by using Cu Kα radiation and a 2θ scan rate of $2^\circ\,min^{-1}$. UV-Vis DRS was obtained by using a Hitachi U-3010 spectrometer.

2.3. Photoreactor and Light Source. The photocatalytic activities were evaluated by the decomposition of 4-CP when irradiated with UV ($\lambda = 254$ nm) and Vis light ($\lambda > 420$ nm). UV light was obtained by a 12 W Hg lamp (Institute of Electric Light Source, Beijing) and the average light intensity was $150\,\mu W.cm^{-2}$. In the case of Vis light irradiation, a 500 W xenon lamp (Institute of Electric Light Source, Beijing) was focused through a window, as a 420 nm cutoff filter was placed onto the window face of the cell to ensure the desired irradiation light. The average light intensity was $30\,mW.cm^{-2}$. The irradiation area was approximately $40\,cm^2$. The radiant flux was measured with a power meter from the Institute of Electric Light Source (Beijing, China).

2.4. Procedures and Analyses. Aqueous suspensions of 4-CP (usually 100 mL, $10\,mg\,L^{-1}$) and 0.1 g of the catalysts were placed in a vessel. Prior to irradiation, the suspensions were magnetically stirred in the dark for ca. 30 min to ensure the establishment of an adsorption/desorption equilibrium. The suspensions were kept under constant air-equilibrated conditions before and during the irradiation. At given time intervals, 3 mL aliquots were sampled and centrifugated to remove the particles. The filtrates were analyzed by recording variations in the absorption band (224 nm) in the UV-Vis

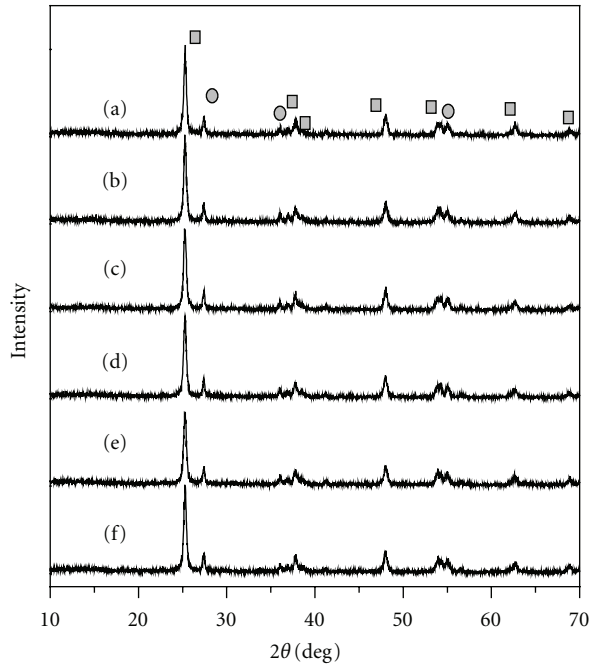

Figure 1: XRD patterns of the N-doped TiO_2 samples annealed under NH3 flow for different time; (a) 0 min, (b) 5 min, (c) 10 min, (d) 15 min, (e) 20 min, (f) 25 min; the anatase (□) and the rutile (○).

spectra of 4-CP using a Hitachi U-3010 spectroscopy. The intermediate products in the filtered sample were determined by a Hewlett-Packard HPLC equipped with an UV detector adjusted to 270 nm and the ODS-2 spherisorb column (125 mm length, 4 mm internal diameter, and 5 μm particle diameters). The mobile phase was a mixture of 50 : 50 (v/v) of CH_3OH to deionized water with a flow rate of 1.0 mL min^{-1}.

2.5. ESR Measurements. ESR signals of radicals spin-trapped by DMPO were recorded at ambient temperature on a Brucker ESR 300 E spectrometer: the irradiation source was a Quanta-Ray Nd : YAG pulsed laser system (λ = 355 nm or 532 nm, 10 Hz). The settings for the ESR spectrometer were: center field, 3486.70 G; sweep width, 100 G; microwave frequency, 9.82 GHz; modulation frequency, 100 kHz; power, 5.05 mW. To minimize experimental errors, the same quartz capillary tube was used for all ESR measurements.

3. Results and Discussion

3.1. Sample Characterization. XRD patterns of the as-prepared samples are shown in Figure 1. Degussa P-25 nanopowder sample, though dominantly of the anatase form, also contains some notable contribution from the rutile structure (ratio approximately 3 : 1) [18]. Replacing an O atom with an N atom in TiO_2 does not result in significant structural changes, although the N atom has a larger ion radius (0.171 nm) than that of the O atom (0.132 nm) [24]. Ti–N bond length, 1.964 Å, is only slightly longer than that of Ti–O, 1.942 Å. Therefore, the structural modifications due to the N doping are relatively minor [30]. This could also be understood that the concentration of the doped N atom (given later) might be low to cause a shift.

Global XPS profiles for the as-prepared samples are shown in Figure 2(a). According to XPS spectra, the samples contain only Ti, O, and N atoms. And binding energies for O 1s, Ti 2s, Ti 2p, and C 1s are 533.2, 576.3, 473.5, and 285.0 eV, respectively. Figure 2(b) shows the N 1s spectra of the as-prepared samples. A new peak at 396 eV was observed, which is generally considered as evidence for the presence of Ti–N bonds, suggesting that the oxygen sites were substituted by nitrogen atoms [26]. In contrast, N_2 gas annealed samples did not display a peak at 396 eV. The peak at 400 eV could be ascribed to N atoms from adventitious N_2, NH_3, or N-containing organic compounds adsorbed on the surface [18]. The estimated x values from the XPS spectra were 0.021, 0.029, 0.035, 0.041, and 0.049 for the samples prepared at NH_3 flow for 5, 10, 15, 20, and 25 min, respectively.

Various forms of N-doped TiO_2, including powders, films, and nanoparticles, have been investigated by XPS [17–19, 31–33]. In most cases, a peak at 396~397 eV was detected and attributed to substitutional nitrogen doping given the proximity to the typical binding energy of 397 eV in Ti–N [31]. However, in a few recent papers, this feature was found to be completely absent while the peaks at higher binding energies (399~404 eV) were observed [19, 32]. In some other cases, both features have been observed [17, 24, 33]. Since the peaks for nitrites and nitrates fall at a very high binding energy (407~408 eV), nitrogen species in doped TiO_2 are expected to be in a lower oxidation state [33].

3.2. Photoabsorbance Properties and Band Structures. Figure 3 shows UV-Vis DRS of $TiO_{2-x}N_x$ and TiO_2. Noticeable shifts of the absorption shoulders into the Vis-light region were observed for $TiO_{2-x}N_x$. This absorption shoulder at 400~550 nm is related to the presence of nitrogen since it increases with nitrogen content. Additionally, the absorption edge of new band well agrees with the reported value for the N-doped TiO_2 system [19, 24]. These samples, after they have been doped, are pale-yellow in color, and the colors were darker gradually as x increased whereas the undoped sample is white. The color of the N doping samples are partially due to the bulk reduction of the crystal, because the thermal decomposition of NH_3 on the TiO_2 surface results in the evolution of molecular hydrogen, which reduces the crystal electronically [17]. In addition, the presence of the Vis absorption band indicates that nitrogen penetrates into the single crystal and effectively changes the electronic structure of TiO_2 [17, 26]. TiO_2 is an indirect gap semiconductor, and the band gaps of the $TiO_{2-x}N_x$ and TiO_2 can be estimated from tangent lines in the plots of the square root of the Kubelka-Munk functions against the photon energy [26], as shown in the insert of Figure 3. The tangent lines, which are extrapolated to $\alpha^{1/2} = 0$, indicate the band gaps of $TiO_{2-x}N_x$ and TiO_2 are $E_g = 2.95$ eV.

In the present study, the electronic structure of N-doped TiO_2 was newly investigated by DFT calculations. We optimized the lattice parameters and atomic positions of TiO_2 by minimizing the total energy of anatase structure.

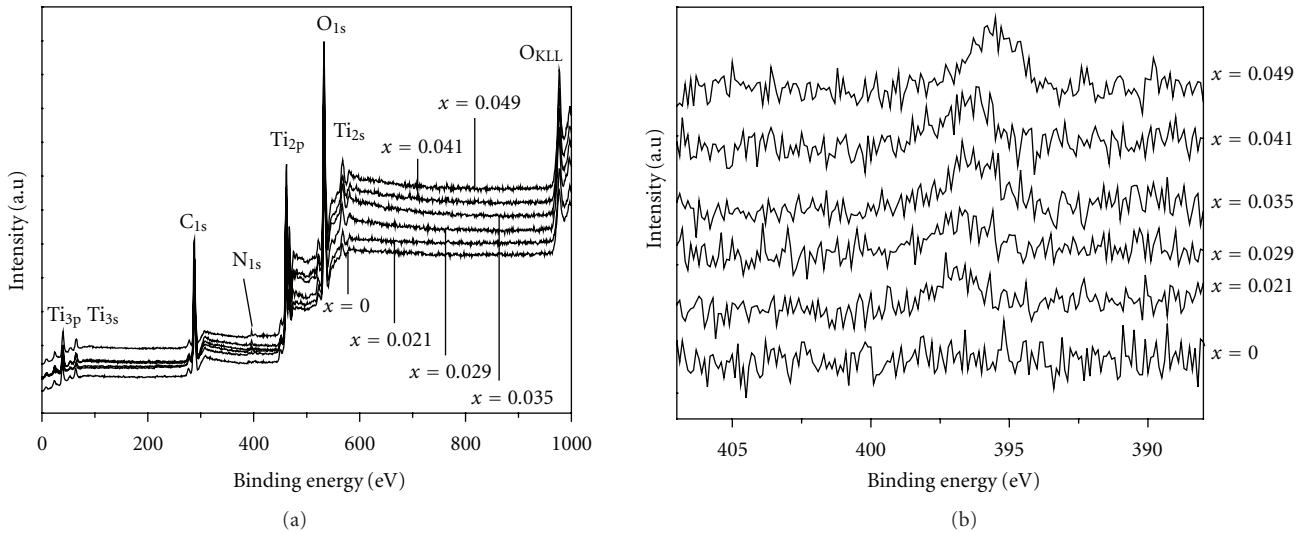

Figure 2: Global XPS of TiO_2-xNx (a), and the N 1s peak of TiO_2-xNx around the 400 eV regions (b).

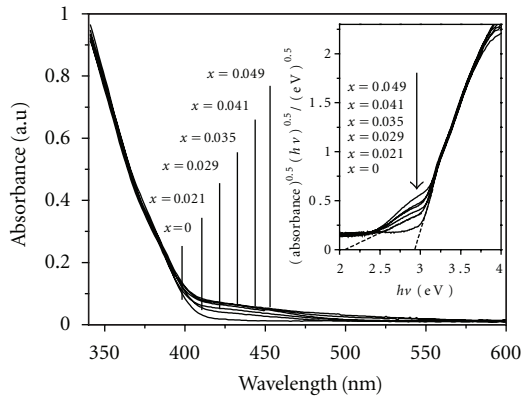

Figure 3: UV-Vis DR spectra of TiO_2-xNx.

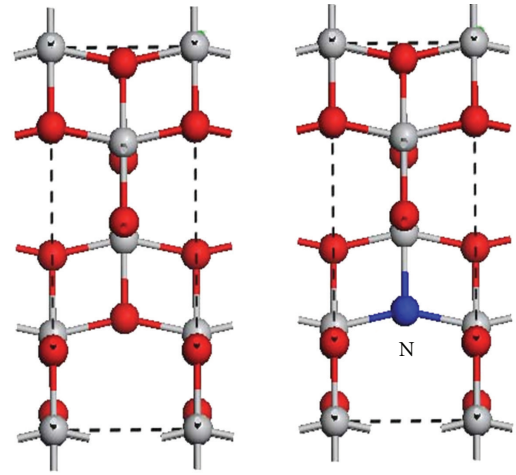

Figure 4: Unit cells of TiO_2 (anatase) (a) and N-doped TiO_2 (b). The red, gray, and blue spheres represent the O, Ti, and N ions, respectively.

The atomic positions of N-doped TiO_2 were optimized based on the theoretical lattice constants of TiO_2 without imposing any symmetry. N doping was modeled by replacing 1 oxygen atoms in the 20-atom anatase supercell, as shown in Figure 4. The resulting stoichiometry is $TiO_{2-x}N_x$ with $x = 0.149$. The DOS results of TiO_2 were shown in Figure 5(a). The occupied bands of TiO_2 were classified into four bands. The lower-energy side in the occupied bands consisted of solely Ti 4s (1~2#). The middle part of the occupied bands consisted of Ti 3p orbitals (3~8#) and O 2s orbitals (9~16#), respectively. The higher-energy side, that is, corresponded to the valence band (VB), consists of O 2p orbitals (13~24#). The bottom of conduction band (CB) was formed by the T 3d orbitals, with a small contribution of the O 2p (25~34#); the top of CB was formed by the Ti 3d orbitals (35~36#). Thus, the highest occupied and lowest unoccupied molecular orbital levels were composed of the O 2p and Ti 3d orbitals, respectively. The band gap of TiO_2 was estimated to be 2.27 eV. Generally, the band gap calculated by DFT is smaller than that obtained experimentally, which is frequently pointed out as a common feature of DFT calculations [34]. The DOS result of N-doped TiO_2 were shown in Figure 5(b). One can see that the VB of N-doped TiO_2 is composed of the hybrid orbitals of O 2p and N 2p. The calculated band gap of TiO_2 was narrowed by 0.41 eV due to the N doping. Asahi et al. calculated by the band structure of $TiO_{2-x}N_x$, where $x = 0.25$ and 0.12, that is, when 12.5 and 6% of the oxygen sites were substituted by nitrogen, and reported that mixing the N 2p and O 2p states narrowed the band gap. The present DOS calculation is in agreement with their conclusion. However, it keenly contradicts with the UV-Vis spectra of N-doped TiO_2 (Figure 3), which showed N-doping did not narrow the band gap of TiO_2 [15].

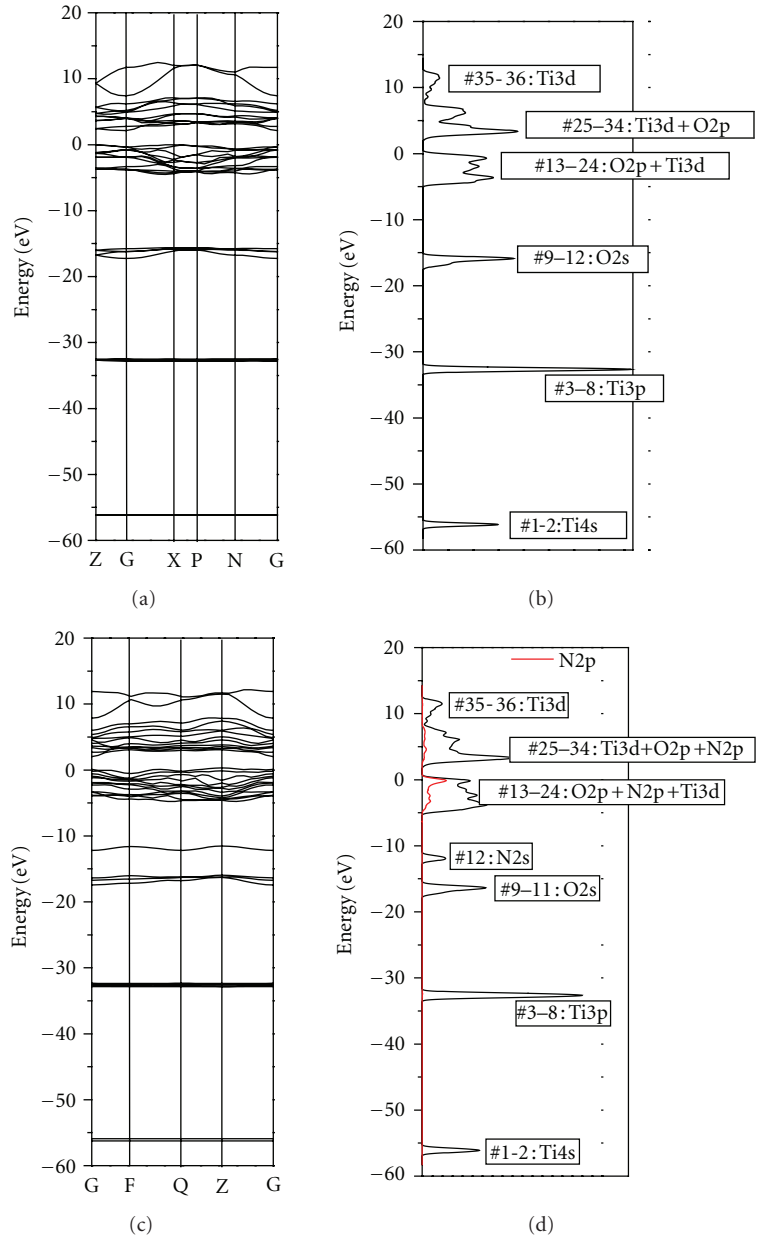

Figure 5: Total DOS: (a) TiO_2 (anatase), (b) N-doped TiO_2.

The procedure of including more N atoms in the same supercell is more accurate than using smaller unit cell as it allows a direct comparison of the various levels of doping on the band structure of the material. Valentin et al. [30] calculated the band gap of $TiO_{2-x}N_x$ with $0.031 < x < 0.094$ by modeling the 96-aom supercell replaced by 1, 2, or 3 nitrogen atoms. Their analysis of the electronic energy levels showed that N doping did not cause the shift of the position of both top and bottom of the O 2p valence band, as well as of the conduction band, with respect to the undoped material. This is in contrast with the conclusion of Asahi et al. [15]. Therefore, the N doping amount could be a vital factor [26]. It is plausible that the band structure of $TiO_{2-x}N_x$ with the lower values of $x < 0.05$ should differ from the higher values of $x > 0.12$.

3.3. Photocatalytic Activity. To explore the photocatalytic activities of the as-prepared samples, the degradation of 4-CP was investigated in both UV and Vis irradiation. 4-CP does not absorb in the Vis region, and therefore the presence of indirect semiconductor photocatalysis can be excluded [19].

Figure 6(a) shows the changes of 4-CP concentration as a function of time in the presence of $TiO_{2-x}N_x$ powders under UV irradiation. The undoped TiO_2 exhibited the highest activity for 4-CP decomposition. 59% loss of 4-CP in concentration was observed in the presence of P-25

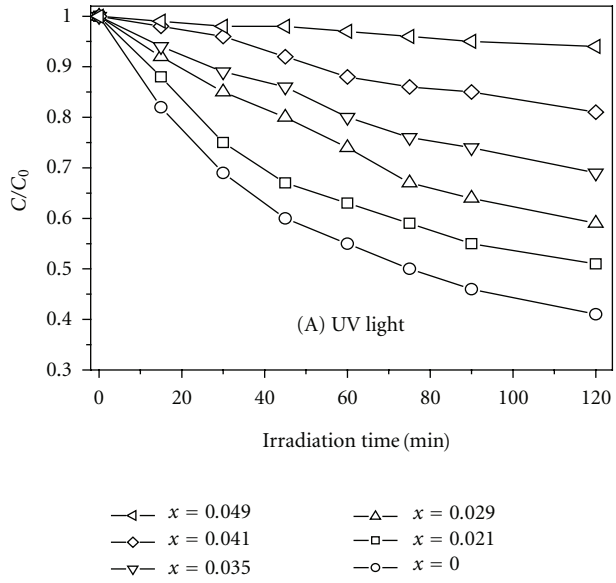

FIGURE 6: Photodecomposition of 4-CP by $TiO_{2-x}N_x$ under UV light (a) and Vis light (b).

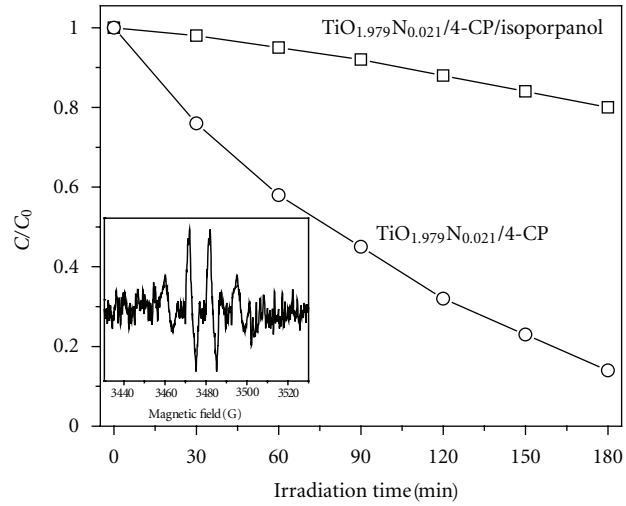

FIGURE 7: Normalized concentration profiles showing 4-CP degradation kinetics upon addition of isopropanol under visible irradiation. Inset: DMPO spin-trapping ESR spectrum under visible irradiation in 4-CP/$TiO_{1.979}N_{0.021}$ aqueous solution. Catalyst loading, 0.5 g L^{-1}; 4-CP, 10 mg L^{-1}; isopropanol, 1×10^{-5} M; the DMPO concentration, 1.6×10^{-2} M.

for 120-minute irradiation. The photocatalytic activity of $TiO_{2-x}N_x$ greatly depended on the concentration of N doping. It is obvious that the photocatalytic activity of $TiO_{2-x}N_x$ decreased as x value increase. 19, 31, 41, and 49% 4-CP were photodegraded in the presence of the sample $x = 0.041$, 0.035, 0.029, and 0.021 for 120 min, respectively. Almost no degradation occurred in the case of the sample $x = 0.049$. It is important to keep or improve UV photoactivity of TiO_2 when it is functionalized for Vis-light-driven catalysis because the most desired solar light source contains about 5% UV and the efficiency of light utilization for a TiO_2-based photocatalyst is much higher for UV than for Vis light [24]. In the present work, the N doping plays a passive role on the UV activity of TiO_2.

Similar experiments were conducted under Vis-light irradiation, as shown in Figure 6(b). Irradiating the undoped TiO_2 ($x = 0$) with Vis light did not generate the decrease of 4-CP in concentration, as TiO_2 is not Vis-light sensitive. The degradation of 4-CP, however, was observed from all the doped samples, suggesting that N-doping for TiO_2 is an effective and feasible approach for achieving Vis-light-driven photocatalysis. As the x value increased, the photoactivity of the sample decreased, which is similar with the case of UV irradiation.

Many factors, for example, surface area, crystallinity, surface hydroxyl density, and oxygen vacancies, affect the activity of a photocatalyst. The activity of a photocatalyst is a combined effect of many factors [24]. In our case, the N-doping concentration dominated these factors because other preparation conditions were identical. Therefore, it is easy to understand that the N-doping concentration in the catalyst could be responsible for the difference of the photoactivity. Irrespective of UV or Vis case, the photoactivies of the N-doped samples decrease with the increase of the N-doping concentration. This is ascribed to the double-faced behaviors of the doped N atoms. The UV-Vis spectra in Figure 3 indicated that the N-doping improved the Vis absorption and increased the number of photons taking part in the photocatalytic reaction. Undoubtedly, this could enhance the photocatalytic activity. On the other hand, they also act as a recombination center of photogenerated charge carriers, and thus deteriorate photocatalysis [26]. The passive role of the N-doped atoms as a recombination center is primary. This was inferred from our results showing a much higher photocatalytic activity is corresponding to the lower x value.

3.4. Formation of Radicals. To probe the nature of the reactive oxygen species generated during the irradiation of the present system, the photodegradation of 4-CP by $TiO_{1.979}N_{0.021}$ in the presence of isopropanol under visible irradiation was performed. The results are shown in Figure 7. It was found that addition of isopropanol, a known scavenger of •OH radicals, prohibited greatly the degradation of 4-CP, indicated that the free •OH radicals were involved in this photoreaction system. The direct evidence of the reactive oxygen species possibly involved in the photodegradation process was examined by EPR technique (DMPO), as shown in the inset of Figure 7. No ESR signals were observed either when 4-CP was absent or when the reaction was performed in the dark in the presence of the catalysts. Under Vis irradiation the characteristic quartet peaks of DMPO-•OH adduct with 1 : 2 : 2 : 1 in the intensity were observed after a 80-second irradiation, which are consistent with the similar spectra reported by others for the •OH adduct [35].

Although the formation of the superoxide radical anion was expected owing to the scavenging of the electrons by O_2, because the N doping did not affect the conduction band of TiO_2 [17], the spin-adduct DMPO-•OOH/O_2•$^-$ was not

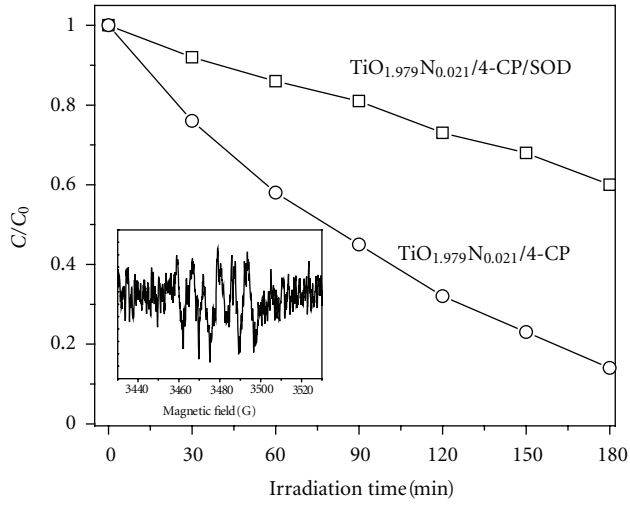

Figure 8: Normalized concentration profiles showing 4-CP degradation kinetics upon addition of SOD under Vis irradiation. Inset: DMPO spin-trapping ESR spectra under Vis irradiation in 4-CP/$TiO_{1.979}N_{0.021}$ ethanol solutions. Catalyst loading, 0.5 g L^{-1}; 4-CP, 10 mg L^{-1}; SOD, 10000 units; the DMPO concentration, 1.6×10^{-2} M.

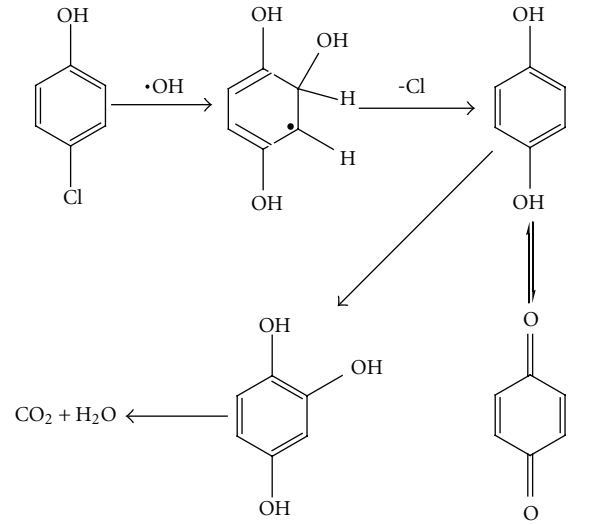

Figure 9: Reaction pathway for the photocatalytic degradation of 4-CP in the presence of $TiO_{1.979}N_{0021}$ under visible irradiation.

detected in the aqueous system. It is well documented that the superoxide radical anions are produced first and remain stable in an organic solvent medium (at least in methanol) [36]. When the fraction of H_2O is increased, such as occurs in a CH_3OH/H_2O mixed solvent system, the superoxide radical anion tends to be unstable, especially in H_2O alone. It is probably because the facile disproportionation reaction of superoxide in water precludes the slow reactions between $\bullet OOH/O_2\bullet^-$ and DMPO ($k = 10$ and $6.6 \times 10^3 M^{-1}s^{-1}$, resp.) [37]. Consequently, we recorded the ESR spectra of the DMPO-$\bullet OOH/O_2\bullet^-$ spin adducts in methanolic media, and the results were as shown in the inset of Figure 8. The six characteristic peaks of $\bullet OOH/O_2\bullet^-$ adducts were observed under Vis irradiation, and the signal intensity increased slightly with irradiation time. No such signals were observed in the dark; that is, generation of $O_2\bullet^-$ anions in the N-doped TiO_2 system inherently implicates irradiation. The effect of superoxide dismutase (SOD) on the 4-CP degradation rate was also observed. The results are shown in Figure 8. The presence of SOD (ca. 10000 units), which catalyzes the dismutation of $O_2\bullet^-$, led to a marked suppression of 4-CP photodegradation. This was in good agreement with the ESR measurement. Kinetics studies by ESR measurements and the radical scavenger techniques clarify that the degradation of visible-light-induced degradation of 4-CP over N-doped TiO_2 is derived mainly by the radical reaction, which is similar to that of TiO_2 under UV light irradiation.

3.5. Proposed Degradation Pathway. During the photocatalytic degradation, the aromatic intermediates were detected by HPLC. The three intermediates generated during the 4-CP degradation are hydroquinone (HQ), hydroxyhydroquinone (HHQ), and benzoquinone (BQ). Figure 9 illustrates the profiles of the intermediated products during the 4-CP degradation using N-doped TiO_2 under Vis-light irradiation.

The initial step is the formation of electron hole pairs on the surface of the catalysts when irradiated by the visible light. The photoinduced electrons at the catalyst surface are scavenged by the ubiquitously present molecular oxygen to yield first O_2^-, whence on protonation yields the HO_2 radicals, and to further produce OH whereas the generated holes can react with hydrated surface of the catalyst, resulting in the formation of surface-bound OH directly. Thus the activated oxygen species, OH, O_2^-, and HO_2 radicals were involved in this photochemical process. However, it is believable that surface-bound and solvated OH radicals are a main oxidant to attack 4-CP. 4-CP is first oxidized into HQ, and then HQ is further oxidized into HHQ and the opening of the ring, and finally the complete mineralization to H_2O and CO_2.

4. Conclusions

$TiO_{2-x}N_x$ ($0.021 < x < 0.049$) has prepared by annealing under an NH_3 flow at 550°C. XRD and XPS confirmed that the so-prepared samples had nitrogen substituted at some of the oxygen sites in TO_2. The Ndoping did not cause the red shift of the absorbed edge of TiO_2 and revealed that the new absorption shoulder at 400~475 nm, suggesting that an isolated narrow band formed above the valence band could be responsible for the Vis light response of the oxynitride powders. The samples showed the photoactivities for the decomposition of 4-CP under both UV and Vis irradiation. When irradiating with UV or Vis light, the activity of the sample decreased with the increase of the N-doping concentration. ESR measurements gave the clear experimental evidence that the active species, such as $\bullet OH$ and $O_2\bullet^-$, generated and participate in the photodegradation of 4-CP over the N-doped TiO_2 catalyst.

Acknowledgments

Financial support was provided by National Natural Science Foundation of China (no. 40975074,20747002) and the Pujiang Talent Program of Shanghai, Doctor project for young teachers of Ministry of Education (20070246028), the Key Laboratory of Industrial Ecology and Environmental Engineering, China Ministry of Education, State Key Laboratory of Pollution Control and Resource Reuse (PCRRF10014).

References

[1] J. Gamage and Z. S. Zhang, "Applications of photocatalytic disinfection," *International Journal of Photoenergy*, vol. 2010, no. 2010, pp. 764870–764881, 2010.

[2] J. Yu, L. Qi, and M. Jaroniec, "Hydrogen production by photocatalytic water splitting over Pt/TiO_2 nanosheets with exposed (001) facets," *Journal of Physical Chemistry C*, vol. 114, no. 30, pp. 13118–13125, 2010.

[3] J. Yu, Y. Hai, and B. Cheng, "Enhanced photocatalytic H_2-production activity of TiO_2 by $Ni(OH)_2$ cluster modification," *Journal of Physical Chemistry C*, vol. 115, no. 11, pp. 4953–4958, 2010.

[4] J. Anthony, P. A. Fernandez-Ibañez, P. S. M. Dunlop, D. M. A. Alrousan, and J. W. J. Hamilton, "Photocatalytic enhancement for solar disinfection of water: a review," *International Journal of Photoenergy*, vol. 2011, no. 2011, pp. 1–12, 2011.

[5] M. L. Chen and W. C. Oh, "The improved photocatalytic properties of methylene blue for $V-_2O_3/CNT/TiO_2$ composite under visible light," *International Journal of Photoenergy*, vol. 2010, pp. 264831–264836, 2010.

[6] B. Naik, K.M. Parida, and C. S. Gopinath, "Facile synthesis of N- and S-incorporated nanocrysalline TiO_2 and direct solar-light-driven photocatalytic acitivity," *Journal of Physical Chemistry C*, vol. 114, pp. 19473–19482, 2010.

[7] W. Choi and S. Kim, "Kinetics and mechanisms of photocatalytic degradation of $(CH_3)_nNH_{4-n}^+$ $(0 \leq n \leq 4)$ in TiO_2 suspension: the role of OH radicals," *Environmental Science and Technology*, vol. 36, no. 9, pp. 2019–2025, 2002.

[8] W. Ho, J. Yu, J. Lin, and P. Li, "Preparation and photocatalytic behavior of MoS_2 and WS_2 nanocluster sensitized TiO_2," *Langmuir*, vol. 20, no. 14, pp. 5865–5869, 2004.

[9] A. Di Paola, S. Ikeda, G. Marcì, B. Ohtani, and L. Palmisano, "Transition metal doped TiO_2: physical properties and photocatalytic behaviour," *International Journal of Photoenergy*, vol. 3, no. 4, pp. 171–176, 2001.

[10] X. Z. Li and F. B. Li, "Study of Au/Au^{3+}-TiO_2 photocatalysts toward visible photooxidation for water and wastewater treatment," *Environmental Science and Technology*, vol. 35, no. 11, pp. 2381–2387, 2001.

[11] E. Bae and W. Choi, "Highly enhanced photoreductive degradation of perchlorinated compounds on dye-sensitized metal/TiO_2 under visible light," *Environmental Science and Technology*, vol. 37, no. 1, pp. 147–152, 2003.

[12] J. J. He, A. Hagfeldt, S. E. Lindquist et al., "Phthalocyanine-sensitized nanostructured TiO_2 electrodes prepared by a novel anchoring method," *Langmuir*, vol. 17, no. 9, pp. 2743–2747, 2001.

[13] W. Zhao, W. Ma, C. Chen, J. Zhao, and Z. Shuai, "Efficient degradation of toxic organic pollutants with $Ni_2O_3/TiO_{2-x}B_x$ under visible irradiation," *Journal of the American Chemical Society*, vol. 126, no. 15, pp. 4782–4783, 2004.

[14] S. Khan, M. Al-Shahry, and W. B. Ingler, "Efficient photochemical water splitting by a chemically modified n-TiO_2," *Science*, vol. 297, no. 5590, pp. 2243–2245, 2002.

[15] K. S. Han, D.K. Lee, and J. W. Lee, "Nature of N 2P, Ti 3d, O 2p hybridization of N-doped TiO_2 nanotubes and superior photovoltaic performatnce through selective atomic N doping," *Chemistry*, vol. 17, no. 9, pp. 2579–2582, 2011.

[16] S. Liu, J. Yu, and W. Wang, "Effects of annealing on the microstructures and photoactivity of fluorinated N-doped TiO_2," *Physical Chemistry Chemical Physics*, vol. 12, no. 38, pp. 12308–12315, 2010.

[17] O. Diwald, T. L. Thompson, T. Zubkov, G. Goralski, S. D. Walck, and J. T. Yates, "Photochemical activity of nitrogen-doped rutile $TiO_2(110)$ in visible light," *Journal of Physical Chemistry B*, vol. 108, no. 19, pp. 6004–6008, 2004.

[18] Q. Xiang, J. Yu, and M. Jaroniec, "Nitrogen and sulfur co-doped TiO_2 nanosheets with exposed {001} facets: synthesis, characterization and visible-light photocatalytic activity," *Physical Chemistry Chemical Physics* , vol. 13, no. 11, pp. 4853–4861, 2010.

[19] S. Sakthivel, M. Janczarek, and H. Kisch, "Visible light activity and photoelectrochemical properties of nitrogen-doped TiO_2," *Journal of Physical Chemistry B*, vol. 108, no. 50, pp. 19384–19387, 2004.

[20] R. Bacsa, J. Kiwi, T. Ohno, P. Albers, and V. Nadtochenko, "Preparation, testing and characterization of doped TiO_2 active in the peroxidation of biomolecules under visible light," *Journal of Physical Chemistry B*, vol. 109, no. 12, pp. 5994–6003, 2005.

[21] X. Hong, Z. Wang, W. Cai et al., "Visible-light-activated nanoparticle photocatalyst of iodine-doped titanium dioxide," *Chemistry of Materials*, vol. 17, no. 6, pp. 1548–1552, 2005.

[22] C. Burda, Y. Lou, X. Chen, A. C. S. Samia, J. Stout, and J. L. Gole, "Enhanced nitrogen doping in TiO_2 nanoparticles," *Nano Letters*, vol. 3, no. 8, pp. 1049–1051, 2003.

[23] G. R. Torres, T. Lindgren, J. Lu, C. G. Granqvist, and S. E. Lindquist, "Photoelectrochemical study of nitrogen-doped titanium dioxide for water oxidation," *Journal of Physical Chemistry B*, vol. 108, no. 19, pp. 5995–6003, 2004.

[24] D. Li, H. Haneda, S. Hishita, and N. Ohashi, "Visible-light-driven N-F-codoped TiO_2 photocatalysts. 1. Synthesis by spray pyrolysis and surface characterization," *Chemistry of Materials*, vol. 17, no. 10, pp. 2588–2595, 2005.

[25] S. U. M. Khan, M. Al-Shahry, and W. B. Ingler Jr., "Efficient photochemical water splitting by a chemically modified n-TiO_2," *Science*, vol. 297, no. 5590, pp. 2243–2245, 2002.

[26] H. Irie, Y. Watanabe, and K. Hashimoto, "Nitrogen-concentration dependence on photocatalytic activity of $TiO_{2-x}N_x$ powders," *Journal of Physical Chemistry B*, vol. 107, no. 23, pp. 5483–5486, 2003.

[27] T. Ihara, M. Miyoshi, Y. Iriyama, O. Matsumoto, and S. Sugihara, "Visible-light-active titanium oxide photocatalyst realized by an oxygen-deficient structure and by nitrogen doping," *Applied Catalysis B*, vol. 42, no. 4, pp. 403–409, 2003.

[28] T. Lindgren, J. M. Mwabora, E. Avandaño et al., "Photoelectrochemical and optical properties of nitrogen doped titanium dioxide films prepared by reactive DC magnetron sputtering," *Journal of Physical Chemistry B*, vol. 107, no. 24, pp. 5709–5716, 2003.

[29] H. Fu, L. Zhang, S. Zhang, Y. Zhu, and J. Zhao, "Electron spin resonance spin-trapping detection of radical intermediates in N-doped TiO_2-assisted photodegradation of 4-chlorophenol," *Journal of Physical Chemistry B*, vol. 110, no. 7, pp. 3061–3065, 2006.

[30] C. D. Valentin, G. Pacchioni, and A. Selloni, "Origin of the different photoactivity of N-doped anatase and rutile TiO_2," *Physical Review B*, vol. 70, no. 8, pp. 1–4, 2004.

[31] O. Diwald, T. L. Thompson, E. G. Goralski, S. D. Walck, and J. T. Yates Jr., "The effect of nitrogen ion implantation on the photoactivity of TiO_2 rutile single crystals," *Journal of Physical Chemistry B*, vol. 108, no. 1, pp. 52–57, 2004.

[32] X. Chen and C. Burda, "Photoelectron spectroscopic investigation of nitrogen-doped titania nanoparticles," *Journal of Physical Chemistry B*, vol. 108, no. 40, pp. 15446–15449, 2004.

[33] C. D. Valentin, G. Pacchioni, A. Selloni, S. Livraghi, and E. Giamello, "Characterization of paramagnetic species in N-doped TiO_2 powders by EPR spectroscopy and DFT calculations," *Journal of Physical Chemistry B*, vol. 109, no. 23, pp. 11414–11419, 2005.

[34] R.M. Dreizler and E. K. Gross, *Density Functional Theory: An Approach to the Quantum Many-Body Problem*, Springer, Berlin, Germany, 1990.

[35] Y. Huang, J. Li, W. Ma, M. Cheng, and J. Zhao, "Efficient H_2O_2 oxidation of organic pollutants catalyzed by supported iron sulfophenylporphyrin under visible light irradiation," *Journal of Physical Chemistry B*, vol. 108, no. 22, pp. 7263–7270, 2004.

[36] C. Chen, W. Zhao, P. Lei, J. Zhao, and N. Serpone, "Photosensitized degradation of dyes in polyoxometalate solutions versus TiO_2 dispersions under visible-light Irradiation: mechanistic implications," *Chemistry*, vol. 10, no. 8, pp. 1956–1965, 2004.

[37] G. Liu, X. Li, and J. Zhao, "Photooxidation pathway of sulforhodamine-B. Dependence on the adsorption mode on TiO_2 exposed to visible light radiation," *Environmental Science and Technology*, vol. 34, no. 18, pp. 3982–3990, 2000.